Comparing the information content of probabilistic representation spaces

Anonymous authors
Paper under double-blind review

Abstract

Probabilistic representation spaces convey information about a dataset, and to understand the effects of factors such as training loss and network architecture, we seek to compare the information content of such spaces. However, most existing methods to compare representation spaces assume representations are points, and neglect the distributional nature of probabilistic representations. Here, instead of building upon point-based measures of comparison, we build upon classic methods from literature on hard clustering. We generalize two information-theoretic methods of comparing hard clustering assignments to be applicable to general probabilistic representation spaces. We then propose a practical method of estimation that is based on fingerprinting a representation space with a sample of the dataset and is applicable when the communicated information is only a handful of bits. With unsupervised disentanglement as a motivating problem, we find information fragments that are repeatedly contained in individual latent dimensions in VAE and InfoGAN ensembles. Then, by comparing the full latent spaces of models, we find highly consistent information content across datasets, methods, and hyperparameters, even though there is often a point during training with substantial variety across repeat runs. Finally, we leverage the differentiability of the proposed method and perform model fusion by synthesizing the information content of multiple weak learners, each incapable of representing the global structure of a dataset. Across the case studies, the direct comparison of information content provides a natural basis for understanding the processing of information.

1 Introduction

The comparison of representation spaces is a problem that has received much attention, particularly as a route to a deeper understanding of information processing systems (Klabunde et al., 2023; Mao et al., 2024; Huh et al., 2024). Existing methods are applicable to point-based representation spaces, including centered kernel alignment (CKA) (Kornblith et al., 2019) and representational similarity analysis (RSA) (Kriegeskorte et al., 2008). For representation spaces whose citizens are probability distributions, such as in variational autoencoders (VAEs) or in biological systems with inherent stochasticity, failure to account for the distributed nature of representations can miss important aspects of the relational structure between data points (Duong et al., 2023). There are surprisingly few options for comparing spaces that fully account for the distributional nature of representations (Klabunde et al., 2023).

One of the only existing methods, stochastic shape metrics (Duong et al., 2023), extends a point-based approach that quantifies the difficulty of aligning one representation space to another through a specified set of allowed transformations (Williams et al., 2021). Here we argue that an information theoretic perspective is most natural when considering the role of a representation space as an intermediate stage of processing in a deep neural network. To be specific, a probabilistic representation space communicates certain information about the data, and we propose to compare two such spaces via quantities related to the mutual information between them. A consequence of focusing on information content is that the spaces can differ in dimensionality, in contrast to shape metrics (Duong et al., 2023), and in whether they are discrete or continuous.

We take as a motivating example the task of unsupervised disentanglement, whose goal is to break information about a dataset into useful pieces. What qualifies as useful depends on the context: although statistical independence between the pieces of information is the predominant desideratum (Locatello et al., 2019), interpretability of the factors can be prioritized (Molnar, 2022) and will clash with independence when correlations are present (Träuble et al., 2021). Other useful properties proposed for disentanglement are compositionality under group operations (Higgins et al., 2018; Balabin et al., 2023) and performance enhancement on downstream tasks (Van Steenkiste et al., 2019).

A significant challenge in disentanglement research is evaluation, which relies on assessing the fragmentation of information about the dataset into channels of a trained model. Models are predominantly evaluated against ground truth factors of variation on overly synthetic datasets (Chen et al., 2018; Kim & Mnih, 2018; Eastwood & Williams, 2018; Hsu et al., 2023). It remains unclear how to evaluate disentanglement when datasets are not accompanied by known generative factors, hindering our understanding of how disentanglement methods work on more realistic datasets. Methods of unsupervised evaluation have been proposed based on a notion of model centrality (Duan et al., 2020; Lin et al., 2020): models that split information similarly to other models are presumed disentangled. Yet, relatedness has failed to account for the probabilistic nature of the representation spaces of the models. Instead, posterior distributions are reduced to points by taking the means of posterior distributions or sampling, and then point-based comparisons such as correlation are applied (Duan et al., 2020).

In this work, we treat probabilistic representation spaces as soft clustering assignments of data, whereby partial distinguishability between data points is expressed by the overlap between posterior distributions. We generalize classic information-theoretic measures of similarity between hard clusterings (Fig. 1a) to be applicable to probabilistic representation spaces (Fig. 1b). By comparing the information content of learned representation spaces produced by multiple models in an ensemble, we study the effects of method, training progress, and dataset on information processing.

Our primary contributions are the following:

1. We generalize two classic measures that compare the information content of clusterings for the comparison of probabilistic representation spaces.
2. We propose a lightweight method to assess information content based on fingerprinting each representation space with the distinguishability of a sample from the dataset.
3. We demonstrate model fusion with the representation spaces from a set of weak VAEs, leveraging the differentiability of the method to maximize the similarity of a synthesis space with respect to the set.

2 Related work

The proposed method builds upon classic means of comparing different cluster assignments (clusterings) of a dataset and generalizes them to compare the information content of probabilistic representation spaces. We then use the method to empirically study generative models designed to fragment information about a dataset in a learned latent space, i.e., for unsupervised disentanglement.

2.1 Similarity of clusterings and of representation spaces

The capacity to compare transformations of data produced by different machine learning models enables ensemble learning, a deeper understanding of methodology, and benchmarking (Punera & Ghosh, 2007). Strehl & Ghosh (2002) used outputs of clustering algorithms to perform ensemble learning, based on a measure of similarity between clustering assignments that we will extend in this work: the normalized mutual information (NMI). Referred to as consensus clustering or ensemble clustering, efforts to combine multiple clustering outputs can leverage any of a variety of similarity measures (Wagner & Wagner, 2007; Vinh et al., 2009; 2010; Vega-Pons & Ruiz-Shulcloper, 2011; Huang et al., 2017). Another measure backed by information theory is the variation of information (VI), coined by Meilă (2003) for clusters but recognized as a metric distance between information sources at least twice before (Shannon, 1953; Crutchfield, 1990).

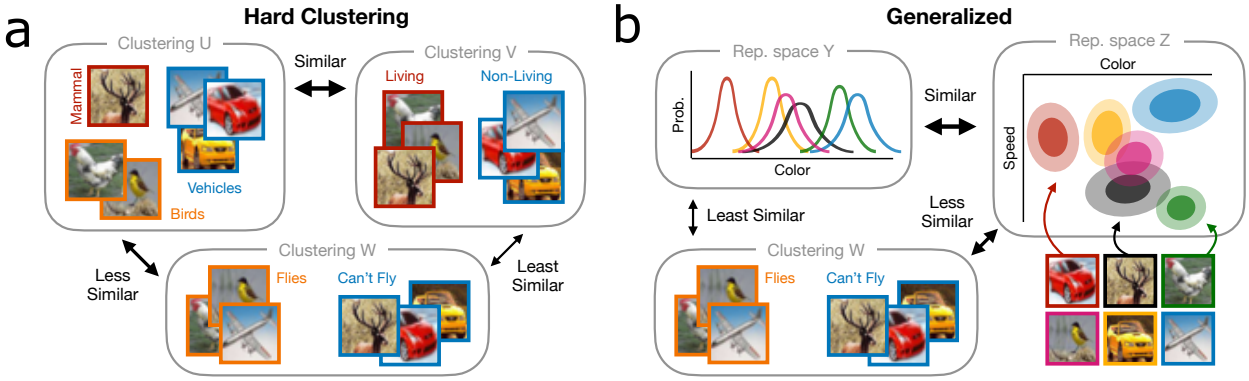

Figure 1: **Similarity of generalized representation spaces. (a)** A hard clustering assignment, such as the living/non-living distinction conveyed by clustering V, communicates certain information about the dataset (here, CIFAR-10 images). Comparing the information content of different clustering assignments enables comparative analyses between algorithms, model fusion, and benchmarking. **(b)** Here we extend measures for hard clusterings to be applicable to generalized representation spaces. There is no requirement for the dimensionality of the spaces to match, and hard clusterings can be compared to probabilistic spaces.

Commonly referred to simply as 'clustering', *hard* clusterings assign every input datum to one and only one output cluster and have been generalized to multiple forms of *soft* clustering (Campagner et al., 2023). We focus specifically on *fuzzy* clustering, where membership is assigned by degree to multiple clusters and must sum to one for each datum (Zadeh, 1965; Dunn, 1973; Ruspini et al., 2019). Probabilistic representation spaces can be viewed as communicating a soft assignment over latent vectors for each datum, with degree of membership expressed by the posterior distributions. Extensions of hard clustering comparisons to fuzzy clusters have been proposed for measures that only indirectly assess information content by counting agreement of assignments, such as the Rand index (Punera & Ghosh, 2007; Hullermeier et al., 2011; D'Ambrosio et al., 2021; Andrews et al., 2022; Wang et al., 2022). Information-based measures have been extended for specific types of soft clusters (Campagner & Ciucci, 2019; Campagner et al., 2023) but none, to our awareness, for comparing the information content of fuzzy clusterings over a continuous representation space.

A rich area of research compares point-based representation spaces via the pairwise geometric similarity of a common set of data points in the space (Kornblith et al., 2019; Hermann & Lampinen, 2020; Klabunde et al., 2023), building upon representational similarity analysis from neuroscience (Kriegeskorte et al., 2008). Stochastic shape metrics (Duong et al., 2023) are a probabilistic extension to a distance metric between two point-based representation spaces based on aligning one with another through prescribed transformations (Williams et al., 2021). Instead of using point-based methods as our starting point, we build upon hard clustering literature because of the extensive connections with information theory.

2.2 Unsupervised disentanglement

Disentanglement is the problem of splitting information into useful pieces, possibly for interpretability, compositionality, or stronger representations for downstream tasks. Shown to be impossible in the fully unsupervised case (Locatello et al., 2019; Khemakhem et al., 2020), research has moved to investigate how to utilize weak supervision (Khemakhem et al., 2020; Sanchez et al., 2020; Vowels et al., 2020; Murphy et al., 2022) and incorporate inductive biases (Balabin et al., 2023; Chen et al., 2018; Rolinek et al., 2019; Zietlow et al., 2021; Hsu et al., 2024).

A significant challenge for disentanglement is evaluation and model selection when no ground truth is available. When a dataset's generative factors are available for evaluation, models are compared against an idealized disentanglement where the factors are whole and separate in latent dimensions (Chen et al., 2018; Kim & Mnih, 2018) and simply encoded (Eastwood & Williams, 2018; Hsu et al., 2023). However, methods of unsupervised model evaluation are few and limited. Duan et al. (2020) proposed that disentangled models are more similar to each other than are entangled ones, in an ensemble of repeats with different initializations.

They evaluated the similarity between two models with an *ad hoc* function of dimension-wise similarity, which was computed as the rank correlation or the weights of a linear model between embeddings in different one-dimensional spaces. ModelCentrality (Lin et al., 2020) is similar: the model most central in an ensemble is taken to be the most disentangled, with similarity quantified with the FactorVAE score (Kim & Mnih, 2018), where one model's embeddings serve as the labels for another model. PIPE (Estermann & Wattenhofer, 2023) is an unsupervised disentanglement metric that relies on a characterization of the posterior distributions in a single model rather than an ensemble. In this work we shift focus from assessing model similarity to channel similarity, under the premise that the fragmentation of information at the core of disentanglement is more naturally studied via the information fragments themselves.

3 Method

Our goal is to compare the information transmitted about a dataset by different representation spaces, and we will use the comparison of hard clustering assignments (e.g., the output of k-means) as a point of reference. Analogously to hard clustering (Fig. 1a), probabilistic representation spaces communicate a *soft* assignment over embeddings that is expressed by a probability distribution in the representation space for each data point (Fig. 1b).

While the proposed method can be applied to any representation space with probabilistic embeddings, we will focus primarily on variational autoencoders (VAEs) (Kingma & Welling, 2014). Let the random variable X represent a sample $x \sim p(x)$ from the dataset under study. X is transformed by a stochastic encoder parameterized by a neural network to a variable $U = f(X, \epsilon)$, where ϵ is a source of stochasticity. We will make use of two fundamental quantities in information theory (Cover & Thomas, 1999), the entropy of a random variable $H(Z) = \mathbb{E}_{z\sim p(z)}[-\log p(z)]$ and the mutual information between two random variables $I(Y;Z) = H(Y) + H(Z) - H(Y,Z)$. The encoder maps each datapoint x to a posterior distribution in the latent space, $p(u|x)$, and the information passed into U about X is regularized by a variational upper bound (Alemi et al., 2017), the expected Kullback-Leibler (KL) divergence (Cover & Thomas, 1999) between the posterior distributions and an arbitrary prior $r(u)$: $\mathbb{E}_{x\sim p(x)}[D_{\mathrm{KL}}(p(u|x)||r(u))]$. Commonly, the posteriors and the prior are parameterized as normal distributions with diagonal covariance matrices, which will facilitate many of the involved measurements but is not required for the method.

3.1 Comparing representation spaces as soft clusterings

Consider a *hard* clustering of data as communicating certain information about the data (Fig. 1a). By observing the cluster assignment U instead of a sample X from the dataset, information $I(X;U)$ will have been conveyed. For a hard clustering, every data point is assigned unambiguously to a cluster—i.e., $H(U|X) = 0$—which makes the communicated information equal to the entropy of the clustering, $I(X;U) = H(U)$.

Given two hard clustering assignments U and V for the same data X, the mutual information $I(U;V)$ measures the amount of shared information content they express about the data. Previous works have found it useful to relate the mutual information to functions of the entropies $H(U)$ and $H(V)$. Strehl & Ghosh (2002) proposed the normalized mutual information (NMI) as the **ratio** of the **mutual information** and the **geometric mean** of the entropies,

$$\mathrm{NMI}(U,V) = \frac{I(U;V)}{\sqrt{H(U)H(V)}}. \tag{1}$$

Meilă (2003) proposed the variation of information (VI), a metric distance between clusterings that is proportional to the **difference** of the **mutual information** and the **arithmetic mean** of the entropies,

$$\mathrm{VI}(U,V) = -2\left(I(U;V) - \frac{H(U)+H(V)}{2}\right). \tag{2}$$

Soft clustering generalizes hard clustering to allow each datum to have partial membership in multiple clusters, effectively communicating partial distinguishability between data points (Zadeh, 1965; Ruspini et al., 2019)

(Fig. 1b). Here we view a probabilistic representation space as a soft clustering, where a datum's posterior distribution $p(u|x)$ expresses a soft assignment over the points u.

The utility of NMI or VI instead of $I(U;V)$ to compare clustering assignments largely resides in the standardization of their values. For two identical hard clustering assignments, U and U', $\text{NMI}(U,U') = 1$ and $\text{VI}(U,U') = 0$. For identical soft assignments—e.g., two copies of a VAE's encoder—NMI will generally not be 1 and VI will not be zero. In contrast to hard clustering assignments, soft assignments include additional entropy resulting from uncertainty that is separate from the information communicated about the dataset, $H(U) = I(X;U) + H(U|X)$. The entropy terms in Eqns. 1 and 2 that ground the mutual information $I(U;V)$ thus include entropy that is irrelevant to the communicated information. We posit that a natural generalization of NMI and VI replaces the entropy of a clustering assignment with the mutual information between two copies of that assignment: $H(U)$ becomes $I(U;U')$, and similarly for V.

The generalized forms become

$$\text{NMI}(U,V) = \frac{I(U;V)}{\sqrt{I(U;U')I(V;V')}}, \tag{3}$$

and VI becomes

$$\text{VI}(U,V) = -2\left(I(U;V) - \frac{I(U;U') + I(V;V')}{2}\right). \tag{4}$$

The generalization leaves NMI and VI unchanged for hard clustering, where $I(U;U') = H(U)$, and enables the measures to be applied to both soft and hard assignments.

The conditional independence of clustering assignments given the data—i.e., $I(U;V|X) = 0$—allows each mutual information term in Eqns. 3 and 4 to be rewritten with regard to information communicated about the data. Namely, $I(U;V) = I(X;U) + I(X;V) - I(X;U,V)$, and $I(U;U') = 2I(X;U) - I(X;U,U')$. Because we have access to the posterior distributions, it is easier to estimate the mutual information between the data X and a representation space (or a combination thereof) than it is to estimate the information between two representation spaces (Poole et al., 2019).

The extended NMI and VI benefit from the generality of information theory: the information content of two probabilistic representation spaces can be compared regardless of dimensionality or parameterization of posteriors, and a soft clustering can be compared to a hard clustering, whether from a quantized latent space or a discrete labelling process (Fig. 1b).

Finally, we note that the generalized VI is no longer a proper metric, as the triangle inequality is not guaranteed (Appx. C).

3.2 Quick estimation based on fingerprinting a representation space

Mutual information can be challenging and costly to estimate (McAllester & Stratos, 2020), and we will often be interested in computing all pairwise similarities between many spaces. Fortunately our primary interest lies in scenarios that simplify the estimation considerably: we will focus exclusively on representation spaces whose members are Gaussian distributions, and often the points of comparison will be individual channels (dimensions) of a VAE or GAN latent space that convey only a few bits of information.

We can use a measure of statistical similarity between posteriors $p(u|x_1)$ and $p(u|x_2)$ in a given representation space—the Bhattacharyya coefficient (Kailath, 1967), $\text{BC}(p,q) = \int_{\mathcal{Z}} \sqrt{p(z)q(z)}dz$—as a route to quickly "fingerprint" the information content of spaces with the pairwise distinguishability of a sample of data points (Murphy & Bassett, 2023). The BC between two multivariate normal distributions can be efficiently computed in bulk via array operations. Once a matrix $\text{BC}_{ij} \coloneqq \text{BC}(p(u|x_i), p(u|x_j))$ of the pairwise values for a random sample of N datapoints is obtained, a lower bound for the information transmitted by the channel can be estimated with $I(X;U) \geq \frac{1}{N}\sum_i^N \log \frac{1}{N}\sum_j^N \text{BC}_{ij}$ (Kolchinsky & Tracey, 2017) (Appx. B). For fast estimation of the information content of a representation space with respect to a ground truth generative factor, we can treat the labels as an effective hard clustering according to that factor, where BC values are either zero or one. Finally, the matrix BC_{ij} for the combination of spaces U_1 and U_2 is their elementwise product. In other words, receiving both of the messages from U_1 and U_2 leads to a distinguishability between data points,

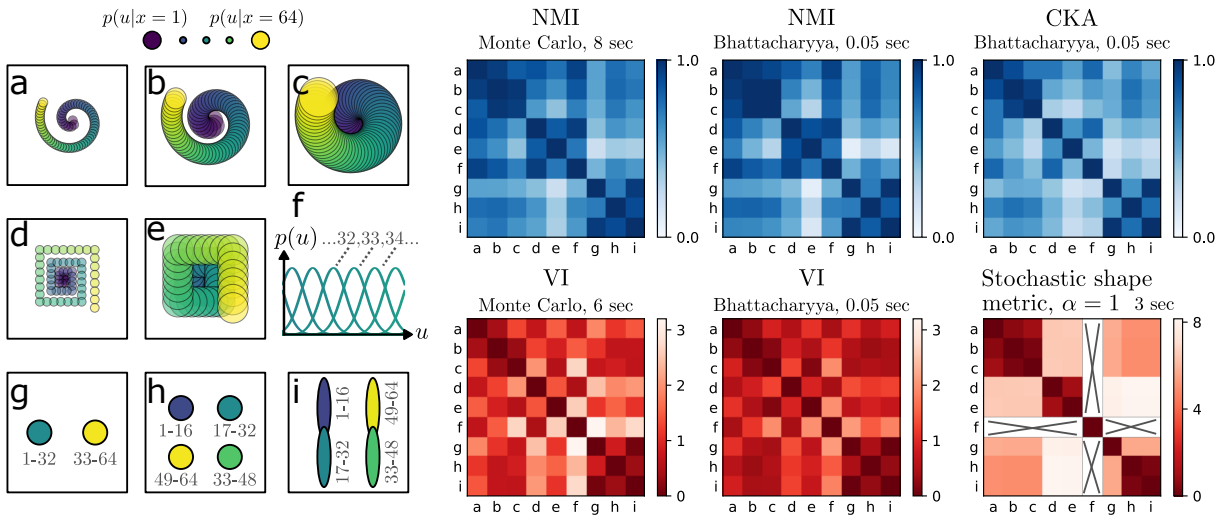

Figure 2: **Comparing similarity measures for synthetic embedding spaces.** *Left:* A dataset of 64 points, $x = 1, ..., 64$, is transformed into nine representation spaces marked **a-i**. Each posterior distribution $p(u|x)$ is a Gaussian with diagonal covariance matrix and standard deviations indicated by the colored ellipses. *Right:* Pairwise similarity (blue matrices) and pairwise distances (red matrices) for generalized NMI, VI, and CKA, derived using either Monte Carlo or the Bhattacharyya fingerprint, and stochastic shape metrics from Duong et al. (2023). Runtimes to calculate the full matrix are shown above each method. The stochastic shape metric requires the dimensionality of the compared spaces to match; undefined entries comparing a 2D space to space **f** are marked with an X.

as computed by the Bhattacharyya coefficient, that is simply the product of the distinguishabilities under U_1 and U_2 separately. Together, the properties allow us to fingerprint each representation space through Bhattacharyya matrices, and then all subsequent analysis can be done with only the matrices—i.e., without having to load the models into memory again.

3.3 Discovering consistently learned information fragments

In the context of disentanglement, we are interested in the similarity of information contained in individual dimensions across an ensemble of models. We compute the pairwise similarities between all dimensions of all models, and then use density-based clustering to identify information content that is found repeatedly. OPTICS (Ankerst et al., 1999) traverses elements in a set according to proximity and produces a "reachability" profile that is similar to a dendrogram produced by hierarchical clustering but more comprehensible for large sets of points (Sander et al., 2003). Valleys indicate denser regions and natural groupings of elements in the set. The consistency of information fragments in individual latent dimensions can then be visualized with the OPTICS reachability profile, the reordered pairwise similarity matrix—which will show a block diagonal form if the fragments are highly consistent—and the NMI with ground truth generative factors, if available.

3.4 Model fusion

Consider a set of representation spaces found by an ensemble of weak learners. In the spirit of "knowledge reuse" (Strehl & Ghosh, 2002) originally applied to ensembles of hard clusters, we might obtain a superior representation space from the synthesis of the set. In contrast to other assessments of representation space similarity (Duan et al., 2020; Kim & Mnih, 2018; Duong et al., 2023), the proposed measures of similarity are composed of mutual information terms, which can be optimized with differentiable operations by a variety of means (Poole et al., 2019). We optimize a synthesis space by maximizing its average similarity with a set of reference spaces, performing gradient descent directly on the encoding of the data points used for the Bhattacharyya matrices. Instead of requiring many models to remain in memory during training of a new

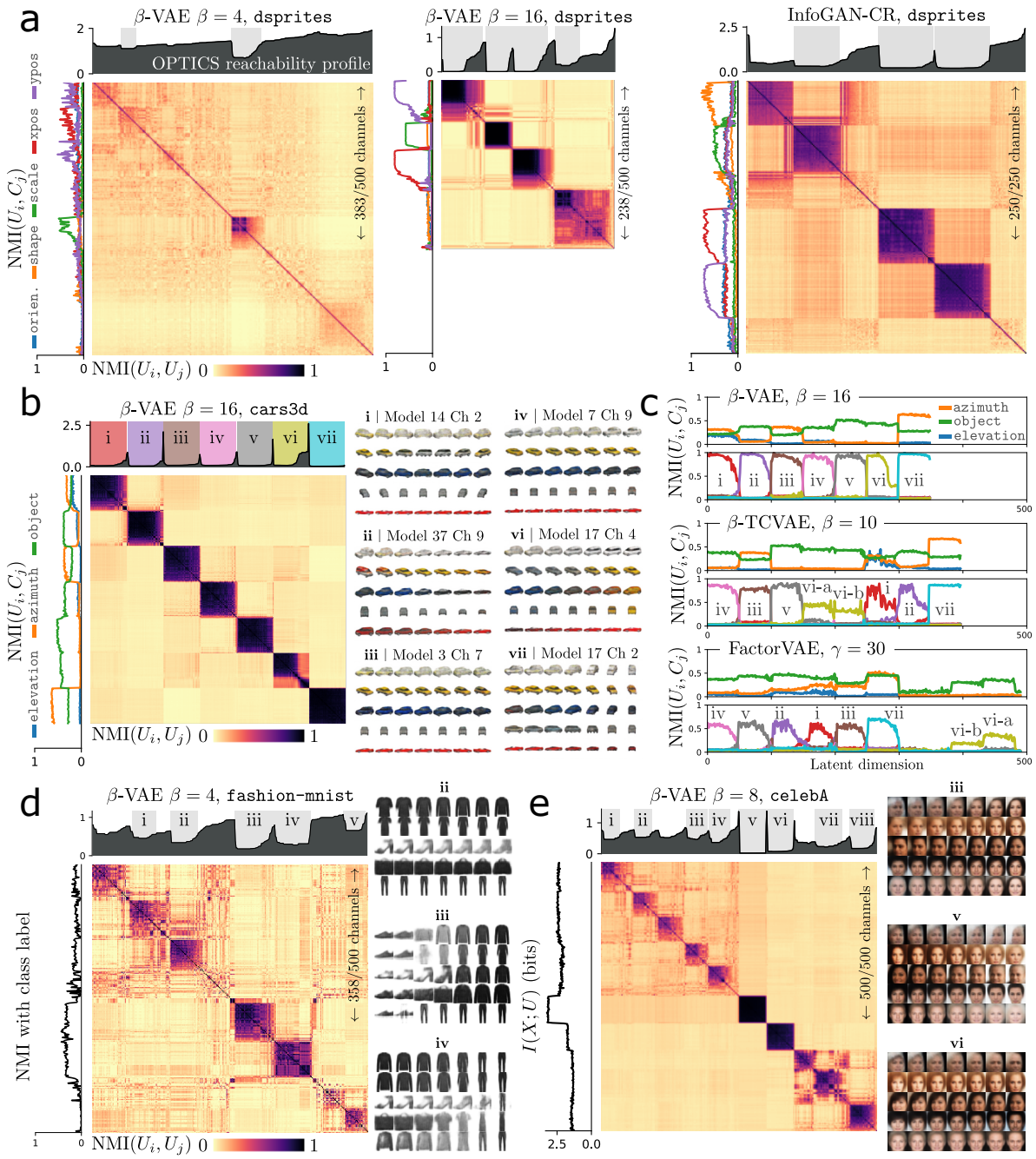

Figure 3: **Channel similarity of ensembles of fifty models. (a)** The channel similarity found in ensembles of models on `dsprites`, for β-VAE and InfoGAN-CR. **(b)** For a β-VAE ensemble trained on `cars3d`, we retrieve the most central representation subspace to each cluster and perform latent traversals. Grouping v can be found in Appx. A. **(c)** We repeat the analysis for β-TCVAE and FactorVAE, and compare the information content of the reordered channels to the representatives from panel **b**. **(d,e)** Channel similarity and latent traversals for β-VAEs trained on `fashion-mnist` and `celebA`.

encoder, the Bhattacharyya matrices are computed for the ensemble once and then used for comparison during training, and training is quick because of the involved array operations.

4 Experiments

4.1 Comparison of related methods on synthetic spaces

We first evaluated the similarity of synthetic representation spaces using ours and related methods (Fig. 2). A dataset of 64 points were embedded to one- and two-dimensional representation spaces, and then the pairwise similarities between the spaces were computed. We evaluated NMI and VI with a Monte Carlo approach and the significantly faster Bhattacharyya fingerprint-based approach. We compare to a modification of CKA (Kornblith et al., 2019) that uses the Bhattacharyya matrices as the similarity measure between representations, and to stochastic shape metrics (Duong et al., 2023). For this small dataset, the Bhattacharyya estimates of NMI and VI are nearly the same as the Monte Carlo alternatives while offering a speed up of 100×. CKA and NMI find comparable similarity structure between the spaces; while CKA lacks the information theoretic underpinnings of NMI, it offers an easy-to-use alternative by simply replacing a point-based distance with a statistical distance between representations. NMI and VI largely agree, though not always: representation space **c** is more similar to space **f** than space **e** according to NMI, and the reverse is true for VI. The magnitude of VI is tied to the magnitude of transmitted information, so when the information of the spaces drops, VI will uniformly assign high similarity. NMI is less dependent on the magnitude of communicated information, though it becomes more sensitive to the uncertainty of information estimates when magnitudes are small (discussed below).

All methods except stochastic shape metrics detect the similarity of the quasi-one-dimensional encodings (representation spaces **a**, **d**, and **f**). These encodings are not related by simple transformations, though a downstream neural network would be able to extract similar information from each. Representation spaces **g** and **i** are similar by information content, as variations of splitting the data into two groups, but they are deemed different by stochastic shape metrics. While stochastic shape metrics satisfy the desirable properties of a metric, the generalized NMI/VI offer a more flexible sense of similarity, owing to their utilization of mutual information.

4.2 Unsupervised detection of structure: channel similarity

We next analyzed the consistency of information fragmentation in ensembles of generative models trained on image datasets. Every latent dimension (channel) of every model in an ensemble was compared pairwise to every other; we used the Bhattacharyya fingerprint approach with a sample size of 1000 images randomly selected from the training set. Before using OPTICS to group latent dimensions by similarity, we removed dimensions transmitting less than 0.01 bits of information. We found NMI to more successfully detect channels with similar information content, and use it for all results in this section (comparison with VI in Appx. D).

In Fig. 3, the matrices display the pairwise NMI between all informative dimensions in the ensemble, and have been reorganized by OPTICS such that highly similar latent dimensions appear as blocks along the diagonal. On the left of each similarity matrix is the NMI with the ground truth generative factors (or other label information), and above is the reachability profile where identified groupings of repeatedly learned channels are indicated with shading and Roman numerals.

In Fig. 3a, the regularization of a β-VAE is increased for the `dsprites` dataset (Higgins et al., 2017). Although there are more channels that convey information for lower regularization (β=4), there is little discernible structure in the population of channels aside from a group of channels that communicate roughly the same information about `scale`. With $\beta = 16$, a block diagonal structure is found, and channels with the same `xpos`, `ypos`, and `scale` information are found repeatedly across runs in the ensemble. We applied the same analysis to an ensemble of InfoGAN-CR models (Lin et al., 2020), whose models additionally encoded `shape` information consistently. We approximated the latent distribution for an image by first encoding it, then re-generating 256 new images with the predicted latent dimensions fixed and the remaining (unconstrained) dimensions randomly resampled, and finally using the moments of the newly predicted latent representations as parameters for a Gaussian distribution. We note that in any scenario where a natural probability distribution exists per datum in the representation space, the method can be used.

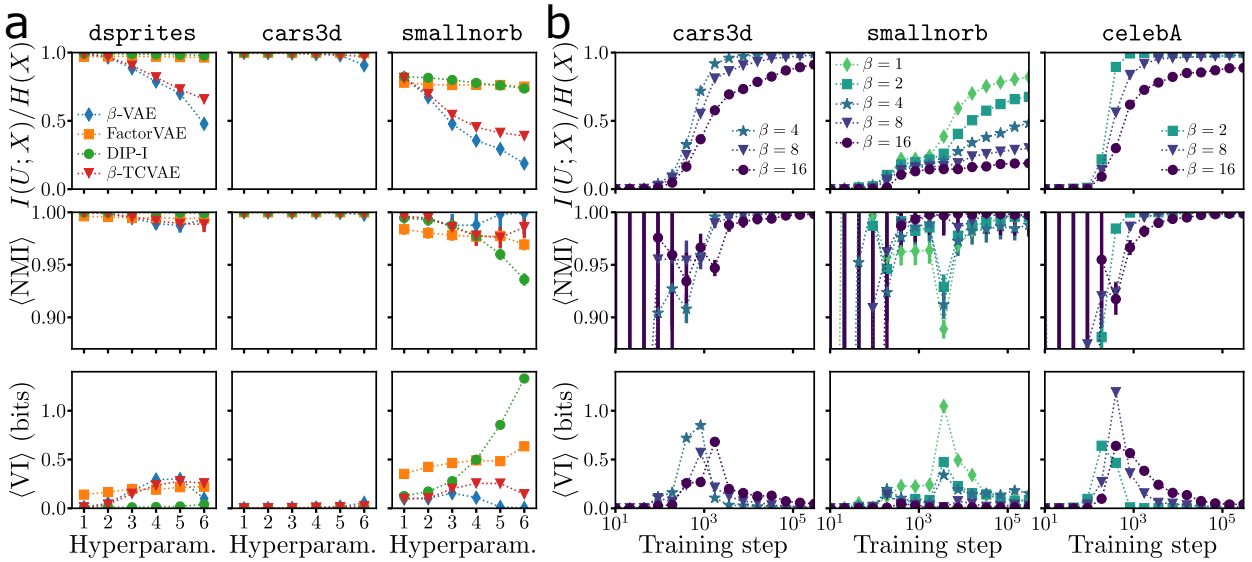

Figure 4: **Comparing full latent spaces. (a)** We compare trained models across several methods and six hyperparameters each, all from Locatello et al. (2019). **(b)** We compare β-VAE models over the course of training. $I(U;X)/H(X)$ is the fraction of total information about the dataset contained in the latent space; a value of one means all data points are well-separated in the latent space. $\langle NMI \rangle$ and $\langle VI \rangle$ denote the average pairwise NMI and VI values over five models in an ensemble. All mutual information terms were estimated via Monte Carlo, and the displayed error bars are the standard error after accounting for the uncertainty on the constituent mutual information terms.

Fig. 3b shows remarkable consistency of information fragmentation by an ensemble of β-VAEs trained on the `cars3d` dataset (Reed et al., 2015), though **not** with regards to the provided generative factors. The `object` factor is broken repeatedly into the same set of information fragments, which is sensible given that it is a fine-grained factor of variation that comprises many lower-entropy factors such as color and height. More surprising is that three of the fragments contain a mix of camera pose information and `object` information that is consistently learned across the ensemble. The majority of existing disentanglement metrics rely on ground truth generative factors—including the FactorVAE score (Kim & Mnih, 2018), mutual information gap (Chen et al., 2018), DCI (Eastwood & Williams, 2018), and InfoMEC (Hsu et al., 2023)—and would miss the consistency found when comparing the information content of individual latent dimensions.

Given a group of latent dimensions identified by OPTICS, we take as a representative the dimension that maximizes the average similarity to others in the group. Latent traversals visualize the fragmented information: groups **i** and **iii** communicate different partial information about both pose and color, while group **vi** conveys information about the color of the car with no pose information.

Is this particular way of fragmenting information about the `cars3d` dataset reproduced across different methods? In Fig. 3c we compared the information content of the seven representative latent dimensions from the β-VAE ($\beta = 16$) to the OPTICS-reorganized latent dimensions for different methods (β-TCVAE (Chen et al., 2018), $\beta = 10$ and FactorVAE (Kim & Mnih, 2018), $\gamma = 30$). The consistent fragments for the other methods are recognizable from those of the β-VAE ensemble, though interestingly the FactorVAE conveyed comparatively less `azimuth` information in several of the fragments. Channels of group **vi** for the β-VAE jointly encoded information about the tint of the windows and the color of the car, and this information was encoded separately by the β-TCVAE and FactorVAE (traversals in Appx. A).

Finally, we studied the manner of information fragmentation on datasets which are not simply an exhaustive set of combinations of generative factors (Fig. 3d,e). For β-VAE ensembles trained on `fashion-mnist` (Xiao et al., 2017) and `celebA` (Liu et al., 2015), some information fragments are more consistently learned than others. A particular piece of information that distinguishes between shoes and clothing (group **iii**) was

repeatedly learned for `fashion-mnist`; for `celebA`, a remarkably consistent fragment of information conveyed background color (group $\mathbf{v}$). The remaining information was less consistently fragmented across the ensemble.

4.3 Assessing the content of the full latent space

If an ensemble of models fragments information into channels inconsistently (e.g., Fig. 3a), is it because the information content of the full latent space varies across repeated runs? We compared the information contained in the full 10-dimensional latent spaces of five models from each VAE-variant ensemble (Fig. 4). The amount of information was generally too large for estimation via Bhattacharyya matrices, which saturates at the logarithm of the fingerprint size, so we used Monte Carlo estimates of the mutual information (Appx. E). Whereas NMI proved more useful for the channel similarity analysis, VI tended to be more revealing about the heterogeneity of full latent spaces. Due to its normalization, NMI becomes dominated by uncertainty when the information contained in the latent space $I(U;X)$ is small (error bars in Fig. 4 are the propagated uncertainty from the mutual information measurements).

Across several methods and several hyperparameters for each method (Fig. 4a; models were from Locatello et al. (2019)), the information contained in the full latent space was largely consistent over different initializations. For the `cars3d` dataset, the latent spaces nearly all conveyed the full entropy of the dataset, meaning all representations were well-separated for the dataset of almost 18,000 images; consequently, the information content was always highly similar. By contrast, none of the models trained on `smallnorb` contained more than around 80% of the information about the dataset, and the similarity of latent spaces across members of an ensemble was more dependent on method and hyperparameter. The consistency of repeat runs of β-VAE and β-TCVAE was fairly high even though the transmitted information dropped considerably with increasing β; DIP-I (Kumar et al., 2018) showed the opposite behavior, where consistency varied strongly with λ_{od} but transmitted information did not.

How does the consistency of latent space information evolve over the course of training? For β-VAE ensembles, we again compared the full latent spaces for five models with random initializations (Fig. 4b). For all datasets considered (`cars3d`, `smallnorb`, `celebA`), consistency across the models dropped at around the same point in training that total information increased dramatically; after this point, all models encapsulated nearly the same information in their latent spaces up to convergence. Interestingly, the magnitude of the drop in NMI (or increase in VI) was monotonic with β for `smallnorb` while the nonmonotonic trend in consistency found in Fig. 4a was recovered by the end of training.

4.4 Model fusion in a toy example

Finally, we created a toy example to demonstrate the capacity for model fusion with the proposed measures of representation space similarity. Consider a dataset with a single generative factor with SO(2) symmetry, such as an object's hue. Difficulties arise when the global structure of a degree of freedom is incompatible with the latent space (Falorsi et al., 2018; Zhou et al., 2019; Esmaeili et al., 2024). Here we focus on a trivial mismatch to clearly demonstrate the synthesis of information from multiple representation spaces.

We trained an ensemble of β-VAEs, each with a one-dimensional latent space that was insufficient to represent the global structure of the generative factor. Fig. 5a shows an example latent space and its associated Bhattacharyya coefficient distinguishability matrix between posterior distributions. The matrix shows the two flaws in the latent space where similar values of the generative factor have dissimilar representations. Assuming the flaws are randomly distributed from one training run to the next—which need not be true—the fusion of several such latent spaces might yield an improved representation of the generative factor.

We performed gradient descent directly on posterior distributions in a two-dimensional latent space, with the objective to maximize average similarity with the ensemble. Namely, we computed either NMI or the $\exp(-\mathrm{VI})$ using the Bhattacharyya matrix corresponding to the optimizable representations—recalculated every training step—and those of the ensemble. As the ensemble size grew, the synthesized latent space more closely captured the global structure of the generative factor (Fig. 5b,c). We quantify the performance with the continuity metric used in Esmaeili et al. (2024), which was adapted from Falorsi et al. (2018), except that

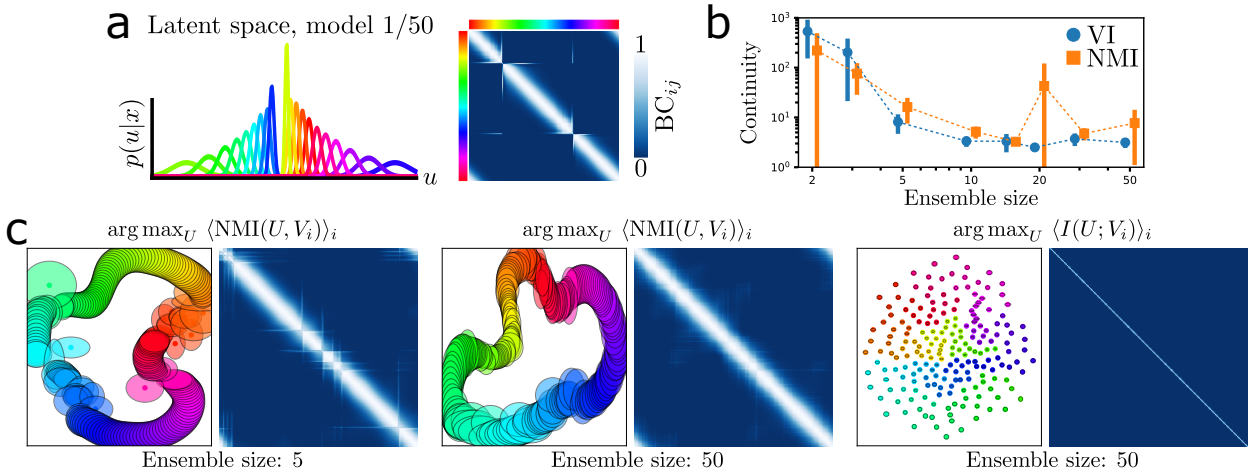

Figure 5: **Learning a factor with $SO(2)$ structure by fusing weak representation spaces. (a)** A one-dimensional latent space of a β-VAE trained on a dataset generated from a single periodic factor that we visualize with color hue. Flaws can be seen in the arrangement of posterior distributions (*left*) and the distinguishability matrix of Bhattacharyya coefficient values between posteriors, BC_{ij} (*right*). **(b)** We optimized a synthesis representation space to have information content that maximizes similarity with an ensemble of one-dimensional spaces such as the one in panel **a**. The continuity of statistical distances between neighboring points, a proxy for the fidelity of the global structure of the generative factor, is shown for VI and NMI with slight horizontal offsets for visibility. Error bars are the standard deviation over five repeats of the experiment. **(c)** Synthesized representation spaces, where posterior means are displayed as points and the covariances as shaded ellipses, and their corresponding distinguishability matrices, where the average NMI (*left*, *middle*) and mutual information (*right*) were maximized.

we used the Bhattacharyya distance between posteriors instead of the Euclidean distance between point-based representations (Appx. E).

Both NMI and VI boosted an ensemble of weak representation spaces to represent the generative factor, and fidelity (as measured by continuity) increased for larger ensembles. By comparison, simply maximizing the average mutual information between the synthesis space and the ensemble (Fig. 5c, right), $\langle I(U; V_i)\rangle_i$, scattered all representations such that $I(X; U) \approx H(X)$. The normalization terms of NMI and VI help to maintain the relational structure between data points. Finally, we note that after training the ensemble of weak models, neither the original data nor the models were needed to train the synthesis space: the latent representations were optimized directly from the Bhattacharyya fingerprints.

5 Discussion

The processing of information can be directly assessed when representation spaces are probabilistic because information theoretic quantities are well-defined. Here we built upon a perspective of probabilistic representation spaces as soft clustering and proposed a natural generalization of two classic measures to compare clustering assignments. Originally, NMI and VI used the entropy of hard clustering assignments to normalize mutual information, but because $H(U) = I(X; U) = I(U; U')$ for a hard clustering U of data X, any of the three quantities could have been used. Only the third quantity, $I(U; U')$, maintains the desirable standardization of NMI $= 1$ and VI $= 0$ for identical soft clustering assignments. By focusing on the information content of a representation space, comparisons are agnostic to aspects of the spaces such as their dimensionality, their discrete or continuous nature, and even whether a space is side information attached to the dataset in the form of labels or annotations (Newman & Clauset, 2016; Savić, 2018; Bazinet et al., 2023).

A more subtle contribution of this work is to shift the current focus of unsupervised disentanglement evaluation. As is clear from the `cars3d` information fragmentation (Fig. 3b), existing metrics that compare

latent dimensions to ground truth generative factors can completely miss consistent information fragmentation. Unsupervised methods of evaluation (Duan et al., 2020; Lin et al., 2020) assess consistency of fragmentation at the scale of models, which can obscure much about the manner of fragmentation. Consider Fig. 3e, where two fragments of information about the `celebA` dataset are significantly more robust than others—what is special about these two pieces of information? We argue that more fine-grained inspection of information fragmentation is essential for a deeper understanding of disentanglement in practice.

The current work largely focused on comparing the information content across repeat training runs in an ensemble, making computational costs an important consideration. We found 50 models per ensemble to be sufficient to assess channel similarity, and only 5 models per ensemble for the full latent space; further, we found that there is still much to learn from ensembles of relatively simple models. On our machine with public code, training a single model from a recently proposed method (QLAE, Hsu et al. (2023)) took more than five hours, whereas we could train ten β-VAEs with a simpler architecture in the same time. Model fusion with weak models that are inexpensive to train, as in Sec. 4.4, might offer a promising alternative to representation learning with more computationally expensive models.

References

Alexander A. Alemi, Ian Fischer, Joshua V. Dillon, and Kevin Murphy. Deep variational information bottleneck. *International Conference on Learning Representations (ICLR)*, 2017. 4

Jeffrey L Andrews, Ryan Browne, and Chelsey D Hvingelby. On assessments of agreement between fuzzy partitions. *Journal of Classification*, 39(2):326–342, 2022. 3

Mihael Ankerst, Markus M Breunig, Hans-Peter Kriegel, and Jörg Sander. Optics: Ordering points to identify the clustering structure. *ACM Sigmod record*, 28(2):49–60, 1999. 6

Nikita Balabin, Daria Voronkova, Ilya Trofimov, Evgeny Burnaev, and Serguei Barannikov. Disentanglement learning via topology. *arXiv preprint arXiv:2308.12696*, 2023. 2, 3

Vincent Bazinet, Justine Y Hansen, and Bratislav Misic. Towards a biologically annotated brain connectome. *Nature reviews neuroscience*, 24(12):747–760, 2023. 11

Andrea Campagner and Davide Ciucci. Orthopartitions and soft clustering: soft mutual information measures for clustering validation. *Knowledge-Based Systems*, 180:51–61, 2019. 3

Andrea Campagner, Davide Ciucci, and Thierry Denœux. A general framework for evaluating and comparing soft clusterings. *Information Sciences*, 623:70–93, 2023. 3

Ricky TQ Chen, Xuechen Li, Roger B Grosse, and David K Duvenaud. Isolating sources of disentanglement in variational autoencoders. *Advances in neural information processing systems*, 31, 2018. 2, 3, 9

Thomas M Cover and Joy A Thomas. *Elements of information theory*. John Wiley & Sons, 1999. 4

James P Crutchfield. Information and its metric. In *Nonlinear Structures in Physical Systems: Pattern Formation, Chaos, and Waves Proceedings of the Second Woodward Conference San Jose State University November 17–18, 1989*, pp. 119–130. Springer, 1990. 2, 23

Sunny Duan, Loic Matthey, Andre Saraiva, Nick Watters, Chris Burgess, Alexander Lerchner, and Irina Higgins. Unsupervised model selection for variational disentangled representation learning. In *International Conference on Learning Representations*, 2020. 2, 3, 6, 12

Joseph C Dunn. A fuzzy relative of the isodata process and its use in detecting compact well-separated clusters. 1973. 3

Lyndon Duong, Jingyang Zhou, Josue Nassar, Jules Berman, Jeroen Olieslagers, and Alex H Williams. Representational dissimilarity metric spaces for stochastic neural networks. In *The Eleventh International Conference on Learning Representations*, 2023. URL https://openreview.net/forum?id=xjb563TH-GH. 1, 3, 6, 8

Antonio D'Ambrosio, Sonia Amodio, Carmela Iorio, Giuseppe Pandolfo, and Roberta Siciliano. Adjusted concordance index: an extensionl of the adjusted rand index to fuzzy partitions. *Journal of Classification*, 38:112–128, 2021. 3

Cian Eastwood and Christopher KI Williams. A framework for the quantitative evaluation of disentangled representations. In *International conference on learning representations*, 2018. 2, 3, 9

Babak Esmaeili, Robin Walters, Heiko Zimmermann, and Jan-Willem van de Meent. Topological obstructions and how to avoid them. *Advances in Neural Information Processing Systems*, 36, 2024. 10, 26

Benjamin Estermann and Roger Wattenhofer. Dava: Disentangling adversarial variational autoencoder. In *International Conference on Learning Representations (ICLR)*, 2023. 4

Luca Falorsi, Pim De Haan, Tim R Davidson, Nicola De Cao, Maurice Weiler, Patrick Forré, and Taco S Cohen. Explorations in homeomorphic variational auto-encoding. *arXiv preprint arXiv:1807.04689*, 2018. 10, 26

Katherine Hermann and Andrew Lampinen. What shapes feature representations? exploring datasets, architectures, and training. *Advances in Neural Information Processing Systems*, 33:9995–10006, 2020. 3

Irina Higgins, Loïc Matthey, Arka Pal, Christopher Burgess, Xavier Glorot, Matthew Botvinick, Shakir Mohamed, and Alexander Lerchner. beta-vae: Learning basic visual concepts with a constrained variational framework. In *International Conference on Learning Representations (ICLR)*, 2017. 8

Irina Higgins, David Amos, David Pfau, Sebastien Racaniere, Loic Matthey, Danilo Rezende, and Alexander Lerchner. Towards a definition of disentangled representations. *arXiv preprint arXiv:1812.02230*, 2018. 2

Kyle Hsu, Will Dorrell, James C. R. Whittington, Jiajun Wu, and Chelsea Finn. Disentanglement via latent quantization. In *Neural Information Processing Systems*, 2023. 2, 3, 9, 12

Kyle Hsu, Jubayer Ibn Hamid, Kaylee Burns, Chelsea Finn, and Jiajun Wu. Tripod: Three complementary inductive biases for disentangled representation learning. *arXiv preprint arXiv:2404.10282*, 2024. 3

Dong Huang, Chang-Dong Wang, and Jian-Huang Lai. Locally weighted ensemble clustering. *IEEE transactions on cybernetics*, 48(5):1460–1473, 2017. 2

Minyoung Huh, Brian Cheung, Tongzhou Wang, and Phillip Isola. The platonic representation hypothesis. *arXiv preprint arXiv:2405.07987*, 2024. 1

Eyke Hullermeier, Maria Rifqi, Sascha Henzgen, and Robin Senge. Comparing fuzzy partitions: A generalization of the rand index and related measures. *IEEE Transactions on Fuzzy Systems*, 20(3):546–556, 2011. 3

Thomas Kailath. The divergence and bhattacharyya distance measures in signal selection. *IEEE transactions on communication technology*, 15(1):52–60, 1967. 5

Ilyes Khemakhem, Diederik Kingma, Ricardo Monti, and Aapo Hyvarinen. Variational autoencoders and nonlinear ica: A unifying framework. In *International Conference on Artificial Intelligence and Statistics*, pp. 2207–2217. PMLR, 2020. 3

Hyunjik Kim and Andriy Mnih. Disentangling by factorising. In *International conference on machine learning*, pp. 2649–2658. PMLR, 2018. 2, 3, 4, 6, 9

Diederik P. Kingma and Max Welling. Auto-encoding variational Bayes. In *International Conference on Learning Representations (ICLR)*, 2014. 4

Max Klabunde, Tobias Schumacher, Markus Strohmaier, and Florian Lemmerich. Similarity of neural network models: A survey of functional and representational measures. *arXiv preprint arXiv:2305.06329*, 2023. 1, 3

Artemy Kolchinsky and Brendan D Tracey. Estimating mixture entropy with pairwise distances. *Entropy*, 19 (7):361, 2017. 5, 22

Simon Kornblith, Mohammad Norouzi, Honglak Lee, and Geoffrey Hinton. Similarity of neural network representations revisited. In *International conference on machine learning*, pp. 3519–3529. PMLR, 2019. 1, 3, 8, 26

Nikolaus Kriegeskorte, Marieke Mur, and Peter A Bandettini. Representational similarity analysis-connecting the branches of systems neuroscience. *Frontiers in systems neuroscience*, 2:249, 2008. 1, 3

Abhishek Kumar, Prasanna Sattigeri, and Avinash Balakrishnan. Variational inference of disentangled latent concepts from unlabeled observations. In *International Conference on Learning Representations*, 2018. URL https://openreview.net/forum?id=H1kG7GZAW. 10

Yann LeCun, Corinna Cortes, and CJ Burges. Mnist handwritten digit database. *ATT Labs [Online]. Available: http://yann.lecun.com/exdb/mnist*, 2, 2010. 17

Zinan Lin, Kiran Thekumparampil, Giulia Fanti, and Sewoong Oh. Infogan-cr and modelcentrality: Self-supervised model training and selection for disentangling gans. In *international conference on machine learning*, pp. 6127–6139. PMLR, 2020. 2, 4, 8, 12, 25

Ziwei Liu, Ping Luo, Xiaogang Wang, and Xiaoou Tang. Deep learning face attributes in the wild. In *ICCV*, pp. 3730–3738. IEEE Computer Society, 2015. ISBN 978-1-4673-8391-2. URL http://dblp.uni-trier.de/db/conf/iccv/iccv2015.html#LiuLWT15. 9

Francesco Locatello, Stefan Bauer, Mario Lucic, Gunnar Raetsch, Sylvain Gelly, Bernhard Schölkopf, and Olivier Bachem. Challenging common assumptions in the unsupervised learning of disentangled representations. In *international conference on machine learning*, pp. 4114–4124. PMLR, 2019. 2, 3, 9, 10, 17, 22, 25

Jialin Mao, Itay Griniasty, Han Kheng Teoh, Rahul Ramesh, Rubing Yang, Mark K Transtrum, James P Sethna, and Pratik Chaudhari. The training process of many deep networks explores the same low-dimensional manifold. *Proceedings of the National Academy of Sciences*, 121(12):e2310002121, 2024. 1

David McAllester and Karl Stratos. Formal limitations on the measurement of mutual information. In *International Conference on Artificial Intelligence and Statistics*, pp. 875–884. PMLR, 2020. 5

Marina Meilă. Comparing clusterings by the variation of information. In *Learning Theory and Kernel Machines: 16th Annual Conference on Learning Theory and 7th Kernel Workshop, COLT/Kernel 2003, Washington, DC, USA, August 24-27, 2003. Proceedings*, pp. 173–187. Springer, 2003. 2, 4

Christoph Molnar. *Interpretable Machine Learning: A Guide for Making Black Box Models Explainable*. 2022. 2

Kieran A Murphy and Dani S. Bassett. Interpretability with full complexity by constraining feature information. In *International Conference on Learning Representations (ICLR)*, 2023. URL https://openreview.net/forum?id=R_OL5mLhsv. 5

Kieran A Murphy, Varun Jampani, Srikumar Ramalingam, and Ameesh Makadia. Learning abcs: Approximate bijective correspondence for isolating factors of variation with weak supervision. In *Proceedings of the IEEE/CVF Conference on Computer Vision and Pattern Recognition*, pp. 16010–16020, 2022. 3

Mark EJ Newman and Aaron Clauset. Structure and inference in annotated networks. *Nature communications*, 7(1):11863, 2016. 11

Ben Poole, Sherjil Ozair, Aaron Van Den Oord, Alex Alemi, and George Tucker. On variational bounds of mutual information. In *International Conference on Machine Learning*, pp. 5171–5180. PMLR, 2019. URL https://proceedings.mlr.press/v97/poole19a/poole19a.pdf. 5, 6

Kunal Punera and Joydeep Ghosh. Soft cluster ensembles. *Advances in fuzzy clustering and its applications*, pp. 69–90, 2007. 2, 3

Scott E Reed, Yi Zhang, Yuting Zhang, and Honglak Lee. Deep visual analogy-making. *Advances in neural information processing systems*, 28, 2015. 9

Michal Rolinek, Dominik Zietlow, and Georg Martius. Variational autoencoders pursue pca directions (by accident). In *Proceedings of the IEEE/CVF Conference on Computer Vision and Pattern Recognition*, pp. 12406–12415, 2019. 3

Enrique H Ruspini, James C Bezdek, and James M Keller. Fuzzy clustering: A historical perspective. *IEEE Computational Intelligence Magazine*, 14(1):45–55, 2019. 3, 4

Eduardo Hugo Sanchez, Mathieu Serrurier, and Mathias Ortner. Learning disentangled representations via mutual information estimation. In *The European Conference on Computer Vision (ECCV)*, 2020. 3

Jörg Sander, Xuejie Qin, Zhiyong Lu, Nan Niu, and Alex Kovarsky. Automatic extraction of clusters from hierarchical clustering representations. In *Advances in Knowledge Discovery and Data Mining: 7th Pacific-Asia Conference, PAKDD 2003, Seoul, Korea, April 30–May 2, 2003 Proceedings 7*, pp. 75–87. Springer, 2003. 6

Miloš Savić. Analysis of annotated social and information networks: Methods and applications. In *Proceedings of the 8th International Conference on Web Intelligence, Mining and Semantics*, pp. 1–4, 2018. 11

Claude Shannon. The lattice theory of information. *Transactions of the IRE professional Group on Information Theory*, 1(1):105–107, 1953. 2

Alexander Strehl and Joydeep Ghosh. Cluster ensembles—a knowledge reuse framework for combining multiple partitions. *Journal of machine learning research*, 3(Dec):583–617, 2002. 2, 4, 6

Frederik Träuble, Elliot Creager, Niki Kilbertus, Francesco Locatello, Andrea Dittadi, Anirudh Goyal, Bernhard Schölkopf, and Stefan Bauer. On disentangled representations learned from correlated data. In *International Conference on Machine Learning*, pp. 10401–10412. PMLR, 2021. 2

Sjoerd Van Steenkiste, Francesco Locatello, Jürgen Schmidhuber, and Olivier Bachem. Are disentangled representations helpful for abstract visual reasoning? *Advances in neural information processing systems*, 32, 2019. 2

Sandro Vega-Pons and José Ruiz-Shulcloper. A survey of clustering ensemble algorithms. *International Journal of Pattern Recognition and Artificial Intelligence*, 25(03):337–372, 2011. 2

Nguyen Xuan Vinh, Julien Epps, and James Bailey. Information theoretic measures for clusterings comparison: is a correction for chance necessary? In *Proceedings of the 26th annual international conference on machine learning*, pp. 1073–1080, 2009. 2

Nguyen Xuan Vinh, Julien Epps, and James Bailey. Information theoretic measures for clusterings comparison: Variants, properties, normalization and correction for chance. *Journal of Machine Learning Research*, 11 (95):2837–2854, 2010. URL http://jmlr.org/papers/v11/vinh10a.html. 2

Matthew J Vowels, Necati Cihan Camgoz, and Richard Bowden. Nestedvae: Isolating common factors via weak supervision. In *Proceedings of the IEEE/CVF Conference on Computer Vision and Pattern Recognition*, pp. 9202–9212, 2020. 3

Silke Wagner and Dorothea Wagner. Comparing clusterings: an overview. 2007. 2

Hong-Yu Wang, Jie-Sheng Wang, and Guan Wang. A survey of fuzzy clustering validity evaluation methods. *Information Sciences*, 618:270–297, 2022. 3

Alex H Williams, Erin Kunz, Simon Kornblith, and Scott Linderman. Generalized shape metrics on neural representations. *Advances in Neural Information Processing Systems*, 34:4738–4750, 2021. 1, 3

Han Xiao, Kashif Rasul, and Roland Vollgraf. Fashion-mnist: a novel image dataset for benchmarking machine learning algorithms. *arXiv preprint arXiv:1708.07747*, 2017. 9

Lotfi Asker Zadeh. Fuzzy sets. *Information and control*, 8(3):338–353, 1965. 3, 4

Yi Zhou, Connelly Barnes, Jingwan Lu, Jimei Yang, and Hao Li. On the continuity of rotation representations in neural networks. In *Proceedings of the IEEE/CVF conference on computer vision and pattern recognition*, pp. 5745–5753, 2019. 10

Dominik Zietlow, Michal Rolinek, and Georg Martius. Demystifying inductive biases for (beta-)vae based architectures. In Marina Meila and Tong Zhang (eds.), *Proceedings of the 38th International Conference on Machine Learning*, volume 139 of *Proceedings of Machine Learning Research*, pp. 12945–12954. PMLR, 18–24 Jul 2021. URL https://proceedings.mlr.press/v139/zietlow21a.html. 3

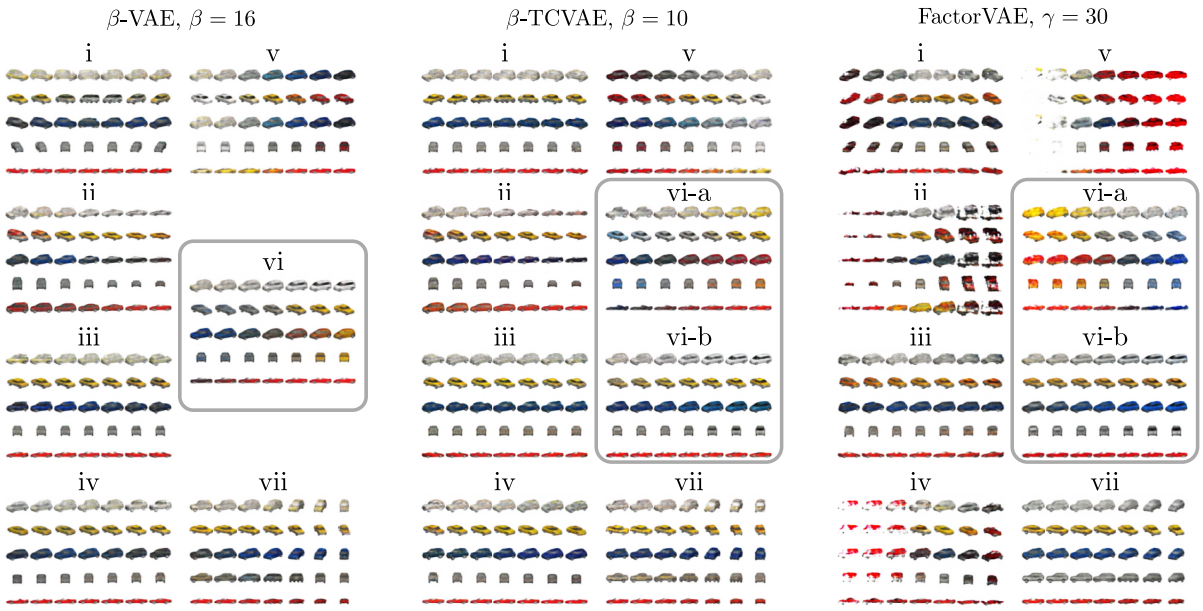

Figure 6: **Latent traversals for `cars3d` groups from Fig. 3b,c.** We traverse the representative channels for the groups found by OPTICS, and reorder them to align with the ordering for β-VAE (left). Note that group **vi** splits in two groups for both the β-TCVAE and the FactorVAE. The tint of the windows and the color of the car were encoded jointly for the β-VAE, and then separately for the other two methods. Traversals are over the range $[-2, 2]$.

A Appendix: Extended channel similarity results

In Fig. 6 we present additional latent traversals for the `cars3d` channel groupings presented in Fig. 3c. With the channels most centrally located in each group (as before), we also display latent traversals for β-TCVAE (β=10) and FactorVAE ($\gamma = 30$).

Fig. 7 visualizes the channel similarity structure on `mnist` (LeCun et al., 2010) and `fashion-mnist`, with latent traversals for four channels per grouping to show the consistency of the encoded information.

In Figs. 8, 9, and 10, we repeat the structural analysis of Sec. 4.2 with all β-VAE hyperparameters explored by the authors of Locatello et al. (2019). The effect of increasing β is clearly observed by the emergence of block diagonal channel similarity matrices, though with fewer informative channels for increased β.

Consider the `cars3d` ensembles in Fig. 8. With $\beta = 1, 2$, the information fragmentation is not consistent across repeat runs, even though the amount of information shared with the three generative factors is fairly consistent. This highlights the value of directly comparing the information content of channels with NMI or VI instead of comparing indirectly via information content about known generative factors, with the added benefit of being fully unsupervised. For $\beta = 4$ the learned fragments of information start to coalesce, with information regularization breaking the degeneracy that plagues unsupervised disentanglement (Locatello et al., 2019). For $\beta = 8, 16$, the regularization is strong enough to form consistent fragments of information across random initializations.

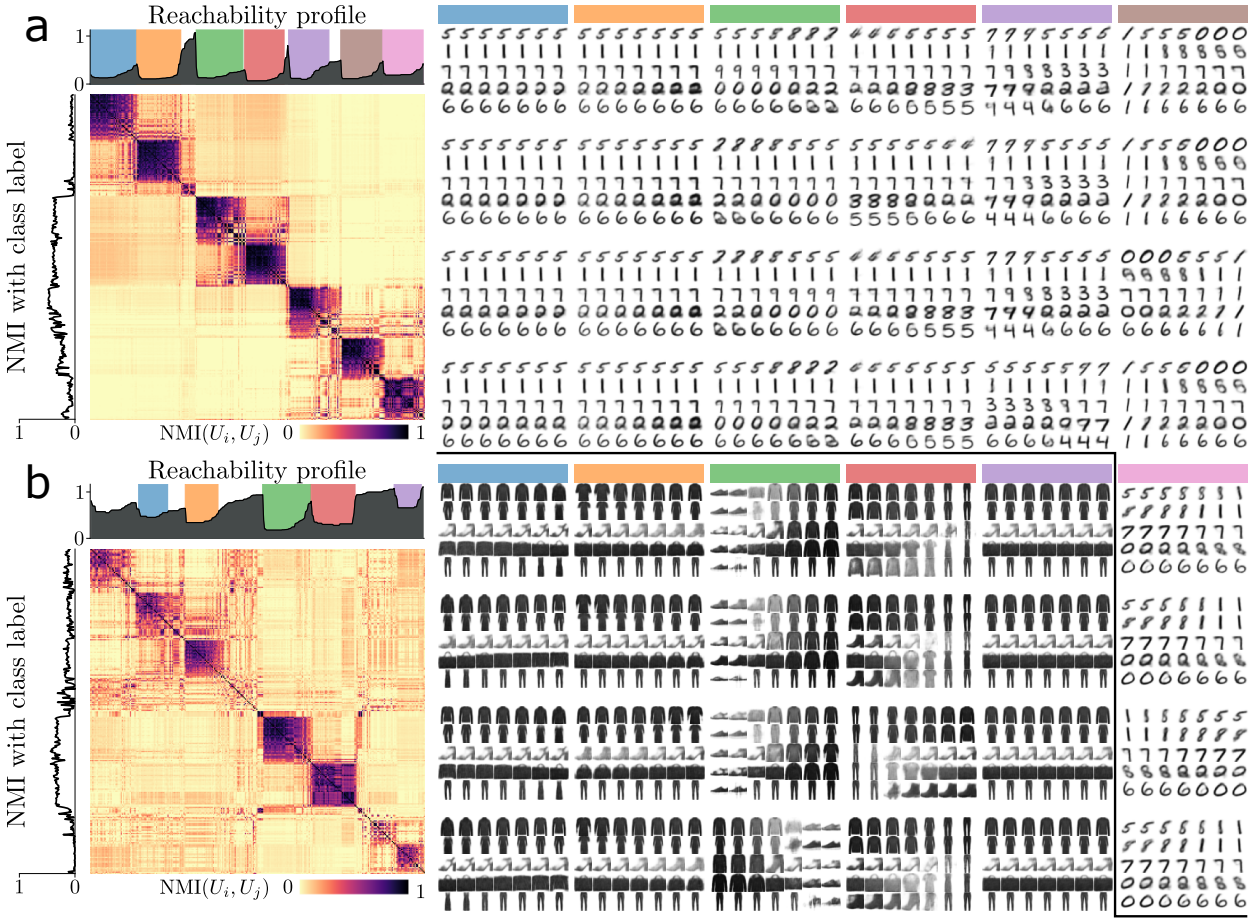

Figure 7: **Channel similarity structure on MNIST and Fashion-MNIST.** Channel similarity analysis for 50 β-VAEs trained on **(a)** MNIST (β=8), and **(b)** Fashion-MNIST ($\beta = 4$). The most central four channels to each of the found groupings (indicated by colors) are visualized via latent traversal on the right.

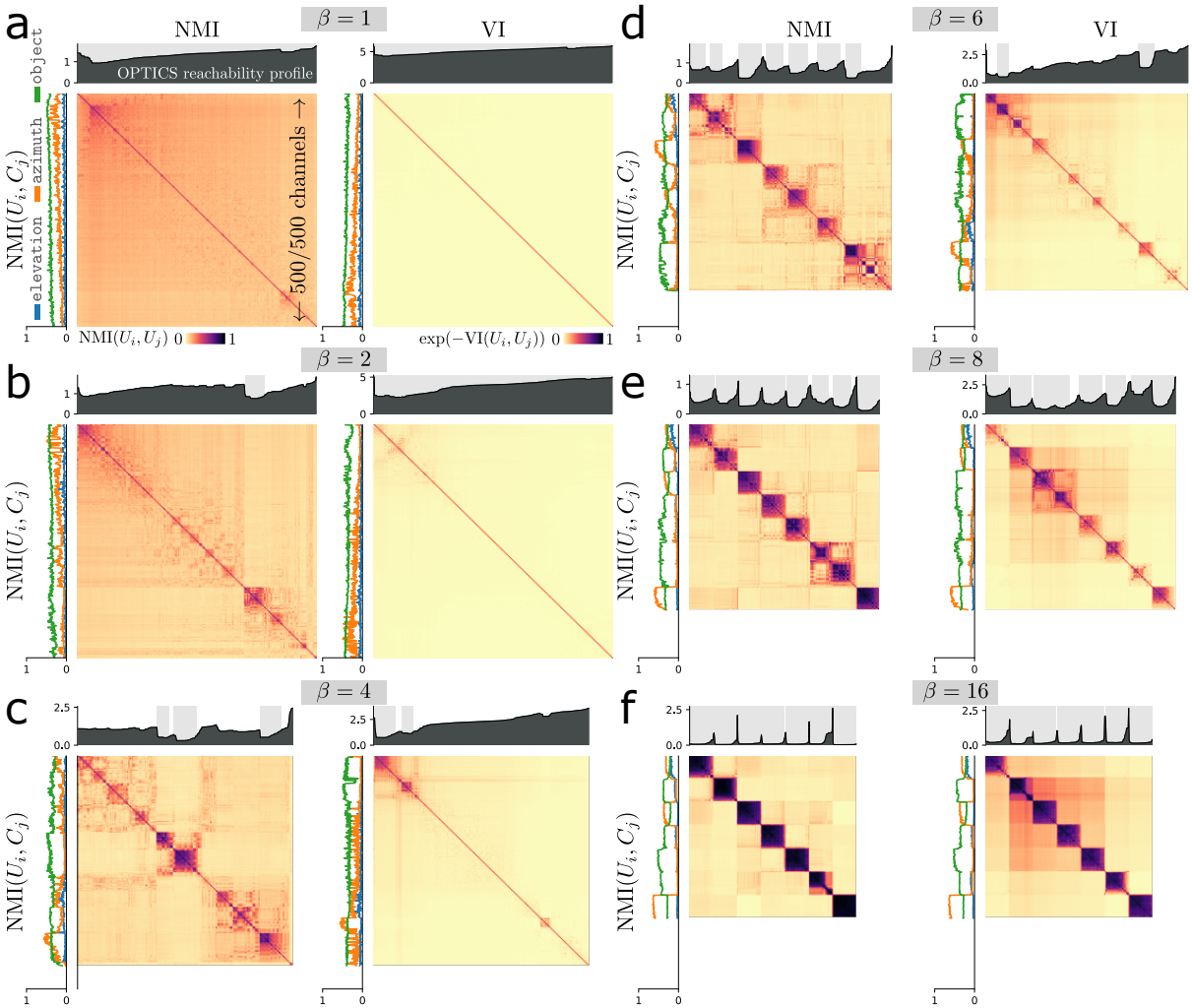

Figure 8: **Channel similarity structure for `cars3d`, β-VAE, assessed with NMI and VI. (a-f)** Ensembles with values of β from 1 to 16, with channels reordered using OPTICS and either NMI (left) or VI (right) for the method of comparison. Regardless of the measure used for comparison, the NMI with the generative factors is shown on the left of each pairwise similarity matrix. All matrices are sized to 500×500, with uninformative channels ($I(U_i; X) \leq 0.01$ bits) displayed as white.

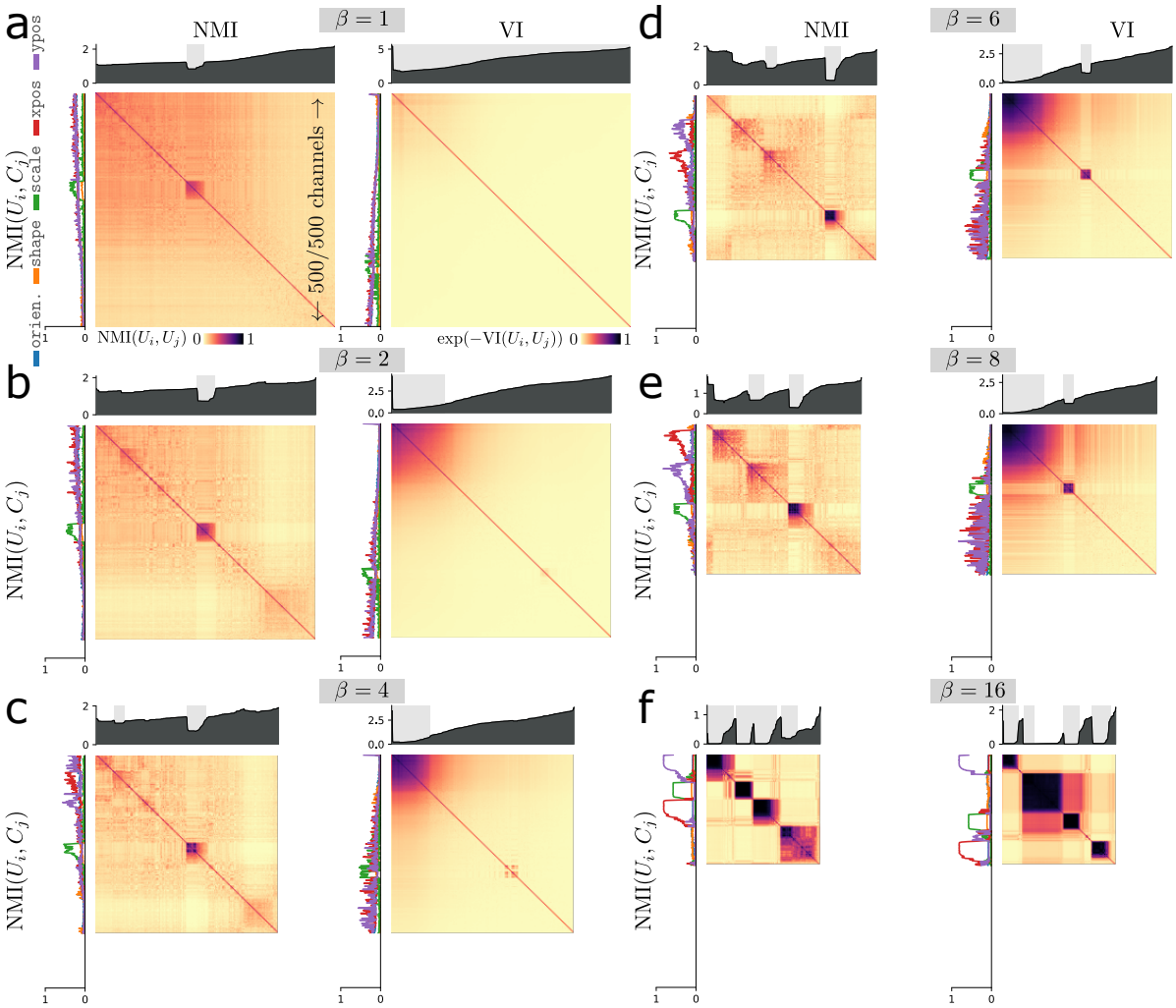

Figure 9: **Channel similarity structure for `dsprites`, β-VAE, assessed with NMI and VI.** Everything in this figure mirrors Fig. 8.

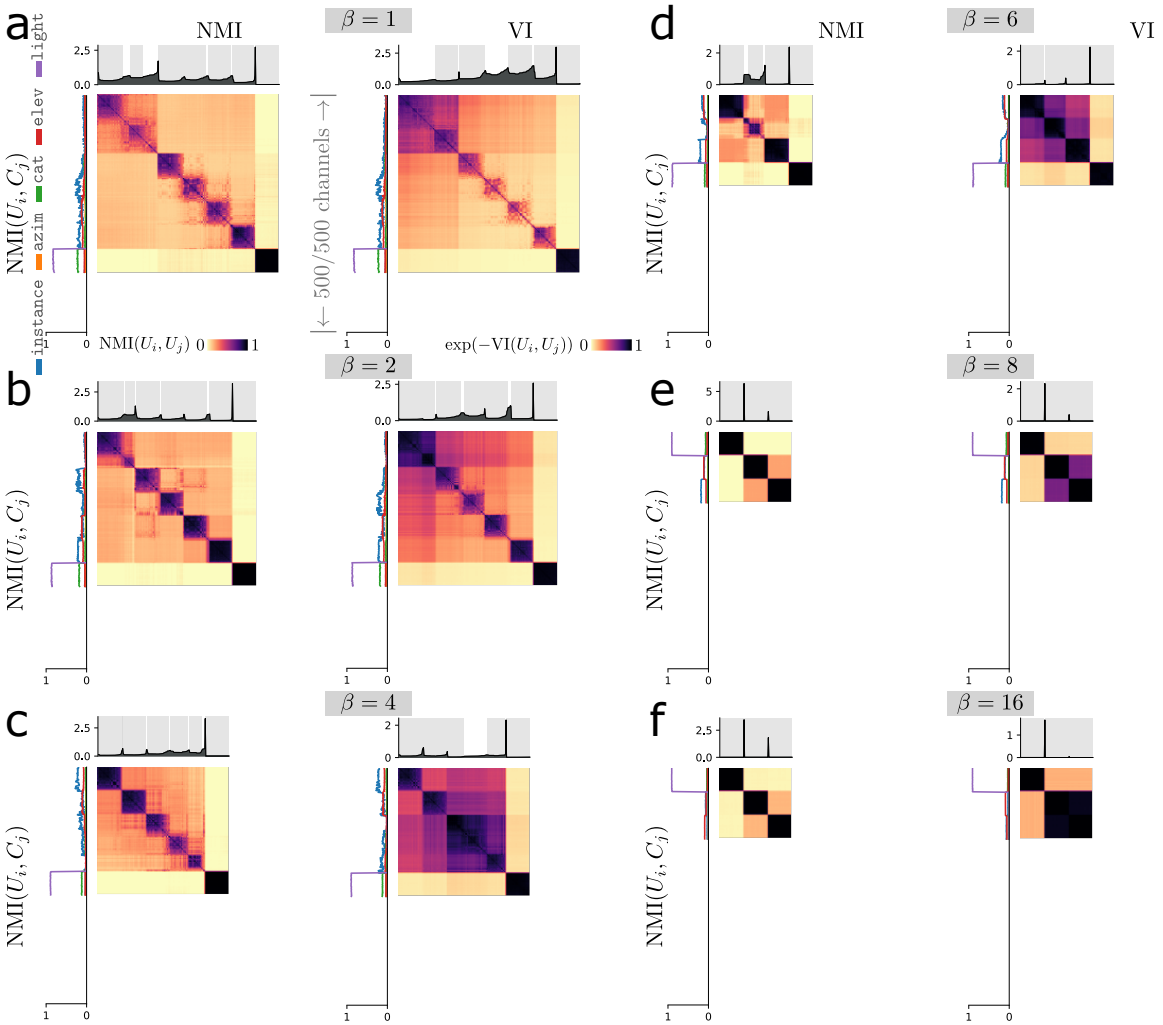

Figure 10: **Channel similarity structure for `smallnorb`, β-VAE, assessed with NMI and VI.** Everything in this figure mirrors Fig. 8.

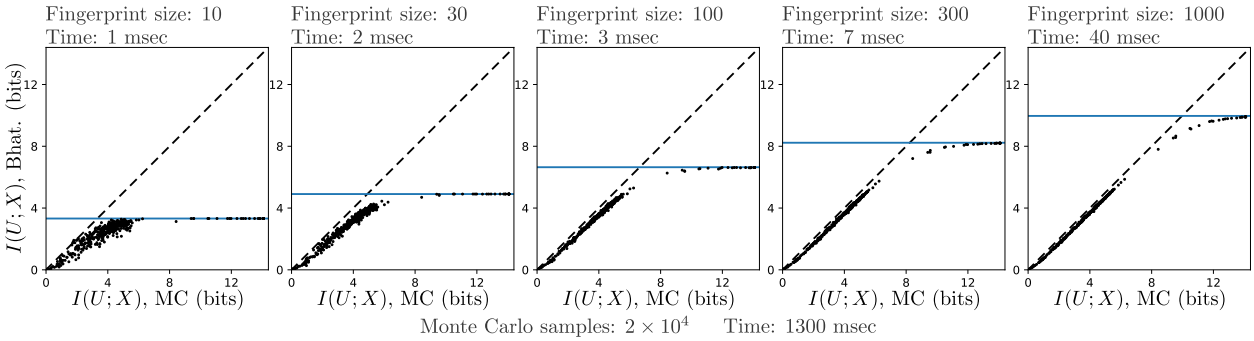

Figure 11: **Information estimates with Bhattacharyya fingerprints and Monte Carlo.** For 500 channels randomly sampled from across all models released by Locatello et al. (2019) for the `cars3d` dataset (including all methods and all hyperparameters), we estimated the amount of information transmitted by each channel $I(U;X)$ using the Bhattacharyya matrix fingerprints and Monte Carlo (MC) sampling. Error bars are displayed for the MC estimates, though they are generally smaller than the markers. The dashed black line represents equality between the two estimates, and the solid blue line is the logarithm of the fingerprint size, which is the saturation point for the Bhattacharyya estimate. Listed run times are for a single channel, excluding the time to load models but including inference and the calculation necessary for $I(U;X)$.

B Appendix: Information estimation using Bhattacharyya distinguishability matrices

To estimate the mutual information $I(U;X)$ from the Bhattacharyya distinguishability matrices, we have employed the lower bound derived in Kolchinsky & Tracey (2017) for the information communicated through a channel about a mixture distribution (following the most updated version on arXiv[1]). The bound simplifies greatly when the empirical distribution is assumed to be a reasonable approximation for the data distribution, and then we further assume the sample of data used for the fingerprint allows for an adequate approximation of the marginal distribution in latent space. First we reproduce the bound from Sec. V of Kolchinsky & Tracey (2017) using the notation of this work, and then we describe our assumptions to apply the bound as an estimate of the information contained in a probabilistic representation space.

Let X be the input to a channel, following a mixture distribution with N components, $x \sim p(x) = \sum_{i=1}^{N} c_i p_i(x)$, and U the output of the same channel, $u \sim p(u) = \sum_{i=1}^{N} c_i \left(\int_{\mathcal{X}} p(u|x) p_i(x) dx\right)$. Then we have

$$I(X;U) \geq -\sum_i c_i \ln \sum_j c_j BC_{ij} + H(U|C) - H(U|X), \tag{5}$$

where C is a random variable representing the component identity.

In this work, we assume that the data distribution can be approximated by the empirical distribution, $p(x) \approx \sum_i^N \delta(x - x_i)/N$, simplifying Eqn. 5 so that $c_i \equiv 1/N$ and $H(U|C) = H(U|X)$ because the identity of the component is equivalent to the identity of the datum. Finally, we assume that the set of posterior distributions for a representative sample of size M of the dataset, taken for the fingerprint, adequately approximates the empirical distribution. Larger samples may be necessary in different scenarios when the amount of information transmitted by channels is larger than a handful of bits, but $M = 1000$ appeared sufficient for the analyses of this work.

The corrections to NMI and VI required the information conveyed by two measurements from different channels, $I(X;U,V)$ as well as from the same channel, $I(X;U,U')$. The matrix of Bhattacharyya coefficients given measurements U and V is simply the elementwise product of the coefficients given U and the coefficients given V. The posterior in the joint space of U and V is factorizable given x—i.e., $p(u,v|x) = p(u|x)p(v|x)$—because the stochasticity in each channel is independent. The same is true for the joint space of U and U',

[1] https://arxiv.org/abs/1706.02419

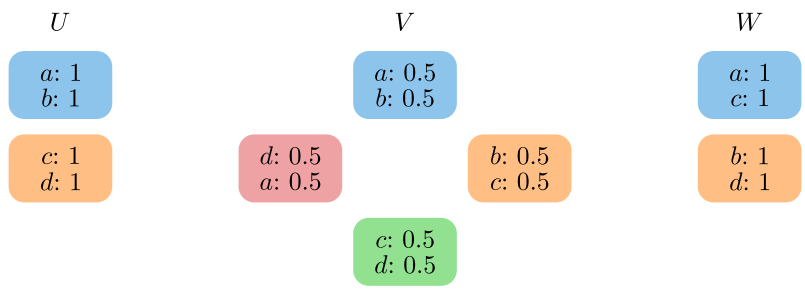

Figure 12: **Example that breaks the triangle inequality for generalized VI.** Four datapoints a, b, c, d are clustered according to scheme U, V, or W. The total VI from U to V and then V to W is less than the VI from U to W.

two draws from the same channel. The Bhattacharyya coefficient of the joint variable simplifies,

$$\begin{aligned} \mathrm{BC}_{ij}^{UV} &= \int_{\mathcal{U}} \int_{\mathcal{V}} \sqrt{p(u,v|x_i)p(u,v|x_j)} du dv \\ &= \int_{\mathcal{U}} \sqrt{p(u|x_i)p(u|x_j)} du \int_{\mathcal{V}} \sqrt{p(v|x_i)p(v|x_j)} dv \\ &= \mathrm{BC}_{ij}^{U} \times \mathrm{BC}_{ij}^{V}. \end{aligned} \tag{6}$$

C Appendix: Broken triangle inequality for the generalized VI

Here we provide an example of three clusterings that breaks the triangle inequality for the generalized VI. Thus, while VI for hard clusters satisfies the properties of a metric (Crutchfield, 1990), the generalization to soft clusters does not.

In Fig. 12, there are three clusterings (U, V, and W) of four equally likely data points ($x \in \{a, b, c, d\}$). U, V, and W each communicate one bit of information about X, but U and W are hard clusterings while V is a soft clustering. We have $I(U;V) = I(V;W) = 0.5$ bits, $I(U;W) = 0$ bits, $I(V;V') = 0.5$ bits, and $I(U;U') = I(W;W') = H(U) = 1$ bit. The generalized VI from U to V and then from V to W is less than from U to W directly.

$$\begin{aligned} \mathrm{VI}(U,W) &= I(U;U') + I(W;W') - 2I(U;W) \\ &= 2 \text{ bits} \\ \mathrm{VI}(U,V) + \mathrm{VI}(V,W) &= 2\Big(I(U;U') + I(V;V') - 2I(U;V)\Big) \\ &= 1 \text{ bit.} \end{aligned}$$

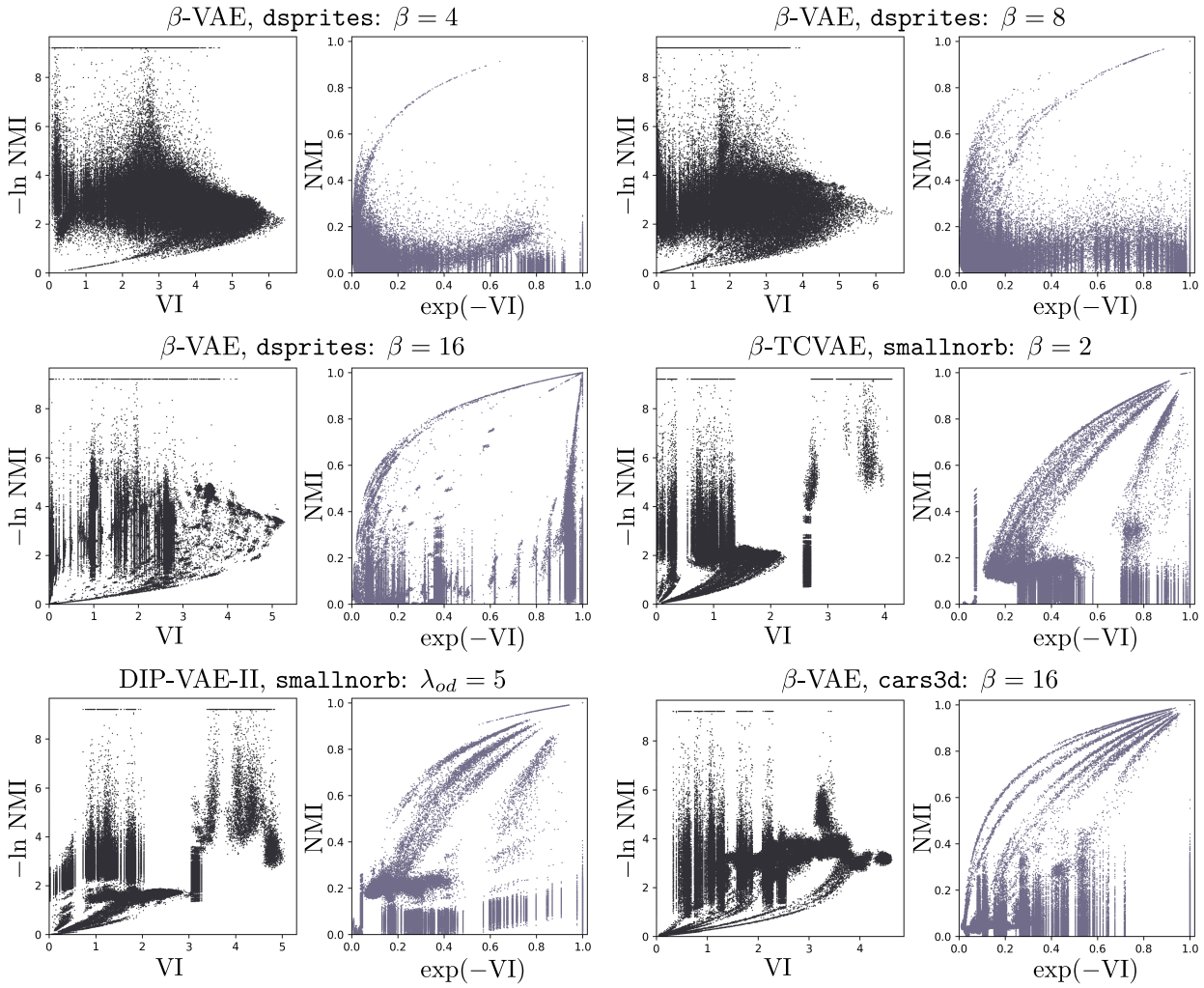

Figure 13: **Direct comparison of NMI and VI.** We convert both measures to a distance measure (black) and to a similarity measure (blue gray) and compare them for the pairwise channel comparisons from the ensembles of Fig. 3.

D Appendix: Are NMI and VI interchangeable?

NMI and VI, aside from the inversion required to convert from similarity to distance, can both be seen as a normalized mutual information. Are they interchangeable, or do they assess structure differently?

In Fig. 13, we compare NMI and VI (estimated via Bhattacharyya matrices) as similarity or distance measures for the pairwise comparisons between channels used in Fig. 3. Specifically, as measures of similarity, we plot NMI against $\exp(-\mathrm{VI})$, and for distance we plot $-\log(\mathrm{NMI})$ against VI. We find that NMI and VI are non-trivially related, shown clearly by the horizontal and vertical swaths of points where one of the two measures is roughly constant while the other varies considerably. Interestingly, the corresponding NMI and VI comparisons in Fig. 13 show multiple distinct arcs of channel similarity, as well as clear vertical bands where NMI has discerning power and VI does not.

E Appendix: Implementation specifics

All experiments were implemented in TensorFlow and run on a single computer with a 12 GB GeForce RTX 3060 GPU.

We have attached code to the submission for the methodological comparisons on the one- and two-dimensional representation spaces of Fig. 2 and ensemble learning of Fig. 5. The heart of the codebase is in `utils.py`, containing the Bhattacharyya and Monte Carlo calculations of $I(U;X)$ and the NMI/VI calculations.

Models: For the `dsprites`, `smallnorb`, and `cars3d` datasets, we used the trained models that were publicly released by the authors of Locatello et al. (2019). Thus, all of the model and channel numbers recorded above the latent traversals in Fig. 3b correspond to models that can be downloaded from that paper's github page[2]. Simply add the model offset corresponding to the $\beta = 16$ β-VAE for `cars3d`, 9250 (e.g., for the traversal labeled with model 31 ch 3, download model 9281 and traverse latent dimension 3, 0 indexed).

For the InfoGAN-CR models on `dsprites`, we used the trained models that were uploaded with Lin et al. (2020)[3].

For results on the training progression of `smallnorb`, `celebA`, and `cars3d`, we used the same architecture and training details from Locatello et al. (2019).

For the MNIST and Fashion-MNIST ensembles, we trained 50 β-VAEs with a 10-dimensional latent space. The encoder had the following architecture:

Conv2D: 32 4×4 `ReLU` kernels, stride 2, padding 'same'

Conv2D: 64 4×4 `ReLU` kernels, stride 2, padding 'same'

Reshape([-1])

Dense: 256 `ReLU`

Dense: 20.

The decoder had the following architecture:

Dense: $7 \times 7 \times 32$ `ReLU`

Reshape([7, 7, 32])

Conv2DTranspose: 64 4×4 `ReLU` kernels, stride 2, padding 'same'

Conv2DTranspose: 32 4×4 `ReLU` kernels, stride 2, padding 'same'

Conv2DTranspose: 1 4×4 `ReLU` kernels, stride 1, padding 'same'.

The models were trained for 2×10^5 steps, with a Bernoulli loss on the pixels, the Adam optimizer with a learning rate of 10^{-4}, and a batch size of 64.

Clustering analysis: We used the OPTICS implementation from `sklearn`[4] with 'precomputed' distance metric and `min_samples`= 20 (and all other parameters their default values). For distance matrices we converted NMI to a distance with $-\log\max(\text{NMI}, 10^{-4})$.

Ensemble learning: For the ensemble learning toy problem (Sec. 4.4), we trained 250 simple β-VAEs (β=0.03) whose encoder and decoder were each fully connected networks with two layers of 256 `tanh` activation. The input was two-dimensional, the latent space was one-dimensional, and the output was two-dimensional.

[2] https://github.com/google-research/disentanglement_lib/tree/master
[3] https://github.com/fjxmlzn/InfoGAN-CR
[4] https://scikit-learn.org/stable/modules/generated/sklearn.cluster.OPTICS.html

The loss was MSE, the optimizer was Adam with learning rate 10^{-3}, and the batch size was 2048, trained for 3000 steps. Data was sampled anew each batch, uniformly at random from the unit circle.

To perform ensemble learning, we evaluated the Bhattacharyya matrices for 200 evenly spaced points around the unit circle for each model in the ensemble. Then we directly optimized the parameters for 200 posterior distributions (Gaussians with diagonal covariance matrices) in a two-dimensional latent space, so as to maximize the average similarity (NMI, exponentiated negative VI, or mutual information) between the Bhattacharyya matrix for the trainable embeddings and those of the ensemble. We used SGD with a learning rate of 3 for 20,000 iterations, and repeated for 5 trials for each ensemble size.

Stochastic shape metrics: We used publicly released code on `github`[5], using the `GaussianStochasticMetric` with $\alpha = 1$ and the parallelized pairwise distances for the timing calculation.

Monte Carlo mutual information estimation: We sampled random data points and then a random embedding vector from each posterior distribution. Then we computed the log ratio of the likelihood under the corresponding posterior and the aggregated posterior (iterating over the entire dataset), and repeated N times to estimate the following expectation:

$$I(X;U) = \mathbb{E}_{x\sim p(x)}\mathbb{E}_{u\sim p(u|x)}\left[\log \frac{p(u|x)}{p(u)}\right] \tag{7}$$

For the analysis of Fig. 4, $N = 2 \times 10^5$ for all datasets except `dsprites` and `celebA`, where $N = 6 \times 10^4$; the standard error of the estimate was on the order of 0.01 bits or less. The displayed points on the plots are weighted means of the values, weighted by the propagated uncertainty on each quantity; the error bars are the standard error of the weighted mean.

CKA: We replaced the dot-product similarity matrices K and L in the Hilbert-Schmidt Independence Criterion (HSIC) with the Bhattacharyya matrices,

$$\mathrm{HSIC}(\mathrm{BC}^{(1)}, \mathrm{BC}^{(2)}) = \frac{1}{(n-1)^2} Tr(\mathrm{BC}^{(1)} \cdot H \cdot \mathrm{BC}^{(2)} \cdot H), \tag{8}$$

and then followed the prescribed normalization in Kornblith et al. (2019).

Continuity metric: Falorsi et al. (2018) used the ratio of neighbor distances in representation space to the corresponding distances in data space, with neighbors taken along continuous paths in data space, as the basis for a discrete continuity metric. It indicated whether any ratios were above some multiplicative factor of some percentile value in the distribution, and thus depended on two parameter choices. Esmaeili et al. (2024) removed one of the parameters—the multiplicative factor—yielding a continuous continuity metric that reports the maximum ratio value over the 90th percentile value.

The central premise of this work is to respect the nature of representations as probability distributions, so we used the Bhattacharyya distance (i.e., $D_{ij} = -\log \mathrm{BC}_{ij}$)) between posteriors instead of Euclidean distances between posterior means in representation space. Other than this modification, we left the continuity metric as in Esmaeili et al. (2024): as the maximum ratio value over the 90th percentile value.

[5] https://github.com/ahwillia/netrep